NIH Public Access
Author Manuscript
Ultrasound Med Biol. Author manuscript; available in PMC 2012 June 1.

Published in final edited form as:
Ultrasound Med Biol. 2011 June ; 37(6): 909–921. doi:10.1016/j.ultrasmedbio.2011.03.001.

Novel Ultrasound and DCE-MRI Analyses after Antiangiogenic Treatment with a Selective VEGF Receptor Inhibitor

Katherine D. Watson[1,2], **Xiaowen Hu**[1], **Chun-Yen Lai**[1], **Heather A. Lindfors**[1], **Dana D. Hu-Lowe**[3], **Theresa A. Tuthill**[5], **David R. Shalinsky**[4], and **Katherine W. Ferrara**[1]

[1]Department of Biomedical Engineering, University of California, Davis

[2]Department of Molecular and Cellular Integrative Physiology, University of California, Davis

[3]Department of Translational Research, Pfizer La Jolla, San Diego, CA

[4]Department of Translational Oncology, Pfizer La Jolla, San Diego, CA

[5]Department of Molecular Medicine, Pfizer New London, Groton CT

Abstract

We report a comparison between tumor perfusion estimates acquired using contrast-enhanced MRI and motion-corrected contrast-enhanced ultrasound before and after treatment with AG-028262, a potent vascular endothelial growth factor receptor tyrosine kinase inhibitor. Antiangiogenic activity was determined by assessing weekly ultrasound and MRI images of rats with bilateral hind flank mammary adenocarcinomas before and after treatment with AG-028262. Images were acquired with a spoiled gradient, 1.5T magnetic resonance sequence and a destruction-replenishment ultrasound protocol. For ultrasound, a time to 80% contrast replenishment was calculated for each tumor voxel; for MR imaging, a measure of local flow rate was estimated from a linear fit of minimum to maximum intensities. AG-028262 significantly decreased tumor growth and increased the time required to replenish tumor voxels with an ultrasound contrast agent from 2.66 to 4.54 seconds and to fill with an MR contrast agent from 29.5 to 50.8 seconds. Measures of flow rate derived from MRI and ultrasound demonstrated a positive linear correlation of r^2=0.86.

Keywords

dynamic contrast-enhanced MRI; destruction-replenishment ultrasound; CPS; VEGF-R; tumor blood flow; perfusion; AG-028262

Introduction and Literature

Tumor growth and metastasis are dependent on angiogenesis to promote cell survival and proliferation. Anti-vascular endothelial growth factor and receptor tyrosine kinase (VEGF, VEGF-RTK) therapies target VEGF binding and signaling, thereby limiting the potent

© 2011 World Federation for Ultrasound in Medicine and Biology. Published by Elsevier Inc. All rights reserved.

Correspondence information: Katherine Ferrara, UC Davis, Department of Biomedical Engineering, 451 Health Sciences Drive, GBSF Room 3311, Davis, Ca 95327, Tel: (530) 754-9436, Fax: (530) 754-5739, kwferrara@ucdavis.edu.

Publisher's Disclaimer: This is a PDF file of an unedited manuscript that has been accepted for publication. As a service to our customers we are providing this early version of the manuscript. The manuscript will undergo copyediting, typesetting, and review of the resulting proof before it is published in its final citable form. Please note that during the production process errors may be discovered which could affect the content, and all legal disclaimers that apply to the journal pertain.

NIH-PA Author Manuscript
NIH-PA Author Manuscript
NIH-PA Author Manuscript

NIH-PA Author Manuscript

NIH-PA Author Manuscript

NIH-PA Author Manuscript

angiogenic effects mediated through VEGF-Rs (Ellis and Reardon 2009). A single anti-VEGF antibody dose can significantly reduce tumor perfusion at 24 and 48 hours after treatment (O'Connor, Carano 2009). The antiangiogenic drug used in this study was AG-028262 (Pfizer, Global Research and Development), which is a potent receptor tyrosine kinase (RTK) inhibitor of VEGF-R1, R2, and R3 autophosphorylation following VEGF stimulation (Zou, Li 2004).

The current imaging standard for tracking antiangiogenic treatment is dynamic contrast enhanced magnetic resonance imaging (DCE-MRI). MRI provides images with great anatomic detail that are important for early detection and diagnosis. However, DCE-MRI is relatively expensive, not widely available, and requires long acquisition times (Padhani and Husband 2001). While advanced MRI scanners have increased temporal resolution capabilities, there are tradeoffs in spatial resolution and/or signal to noise ratio (El Khouli, Macura 2009). Additionally, MRI signal enhancement has a nonlinear dependence on contrast agent concentration at high doses (Elkington, He 2005, Kholmovski and DiBella 2007, Tweedle, Wedeking 1991). Furthermore, MRI estimates of perfusion rates are complicated by the extravasation of MRI contrast agents (Calamante, Vonken 2007, Horsfield, Thornton 2009, Larsson, Stubgaard 1994, O'Connor, Jackson 2007). The use of the Tofts model to estimate DCE-MRI kinetics requires an arterial input function which can be particularly difficult to estimate in small animals (Tofts, Brix 1999, Yankeelov, Cron 2007).

For many applications, ultrasound estimation of blood volume and flow rate is an attractive alternative to MRI flow measurement methods. Contrast enhanced ultrasound (CE-US) is relatively inexpensive on a per-scan basis and has the potential for broad use based on the portability and lower cost of the equipment. Ultrasound contrast agents are microbubbles composed of high-molecular weight gases encapsulated in a protective shell (Chomas, Dayton 2001, Foster, Burns 2000). Harmonic and other nonlinear modes, such as contrast pulse sequencing (CPS), selectively detect the nonlinear echoes produced by ultrasound contrast agents while suppressing the echoes created by tissue (Foster, Burns 2000, Phillips and Gardner 2004). CPS uses a multi-pulse transmission sequence with precise changes in interpulse amplitude and phase (½, -1, ½) to differentiate linear and nonlinear scatterers. CPS has been applied for the qualitative assessment of regional brain and solid organ infarction, liver and renal masses, and response to radiofrequency ablation of tumors in human studies (Bartels, Henning 2005, Bauditz, Schade 2007, von Herbay, Schick 2006, Wink, de la Rosette 2007, Wink, Laguna 2007). The spatial variation in contrast agent density in such images correlates with the tumor morphology and density of viable tumor cells, as estimated by histology using hematoxylin and eosin staining (Broumas, Pollard 2005, Chomas, Pollard 2003).

Sequences of low pressure pulses, such as those used with CPS, have been applied to assess the dynamics of contrast agents in tumor vasculature in pre-clinical and clinical studies. Such dynamics have been shown to change in response to tumor therapies (Lamuraglia, Escudier 2006, Lassau, Brule 2008, Lassau, Chami 2007, Lassau, Chebil 2010, Lassau, Lamuraglia 2006, Magnon, Galaup 2007).

Alternatively, destruction-replenishment ultrasound uses a high pressure pulse of ultrasound to fragment the contrast agent within the imaging plane, followed by a lower pressure, higher frequency, non-destructive pulse to track the replenishment of the intravascular tracer (Chomas, Dayton 2001, Feinstein 2004, Pollard, Dayton 2009, Wei, Jayaweera 1998). When CPS, or another nonlinear imaging method, is integrated with a destructive pulsing sequence, the combined methods can resolve tumor microcirculation and detect low flow rates while maintaining morphologic detail by detecting the replenishment of microbubbles

NIH-PA Author Manuscript

NIH-PA Author Manuscript

NIH-PA Author Manuscript

into the region of interest (Chomas, Pollard 2003, Dayton and Ferrara 2002, Dijkmans, Knaalpen 2004, Foster, Burns 2000, Krix, Plathow 2004, Pollard, Dayton 2009, Potdevin, Fowkes 2004, Wei, Jayaweera 1998, Wei, Le 2001, Wei, Ragosta 2001). The contrast replenishment rate is then quantified by either estimating the volume flow rate (Unger, McCreery 1998, Wei, Ragosta 2001) or the time required for contrast replenishment (Chomas, Pollard 2003). A parametric image of contrast replenishment within a region can then be created, facilitating observations of the varied flow rate across the image (Chomas, Pollard 2003). Each color-encoded pixel represents an estimate of the contrast replenishment rate for a small region (Chomas, Pollard 2003, Yankeelov, Niermann 2006). Depending on the center frequency of the ultrasound imaging pulses, the spatial resolution of each estimate is on the order of hundreds of microns to millimeters.

As with all ultrasound contrast imaging sequences, the use of CPS for the quantification of vascular parameters is compromised by tissue motion. Several tracking techniques have been described; however, many come at a high computational cost directly related to the size of the search region and tracking kernel (Jiang and Hall 2007, Li and Lee 2002, Zhu and Hall 2002). For real-time imaging, the sum absolute difference (SAD) method has been suggested because it is computationally simpler than other algorithms while still performing well in quantitative phantom experiments of motion tracking (Bohs and Trahey 1991). Here, the SAD algorithm is used to align the data within a user-defined box, improving the quantitation of vascular response.

DCE-MRI has been compared to CE-US previously using an MRI-based transport coefficient and CE-US estimate of volume flow rate (Yankeelov, Niermann 2006). Here, we compare an estimate of the time required for ultrasound contrast agent replenishment to MRI-based estimates of contrast agent inflow in order to assess treatment efficacy. We hypothesized that motion-corrected destruction-replenishment CPS ultrasound can be used to monitor antiangiogenic treatment in tumors. To evaluate future clinical applicability we first test whether ultrasound data acquired from different, but similar, planes yields consistent estimates of the therapeutic response. Next, we compare ultrasound contrast replenishment times to the time required for the inflow of an MRI contrast agent. This eliminates the need for further compartmental modeling and permits us to compare measures dominated by perfusion rather than vascular permeability (Harrer, Hornen 2008, Meves, Wilkening 2002, Niermann, Fleischer 2007, Yankeelov, Niermann 2006).

Materials and Methods

Cell Culture

Rat mammary adenocarcinoma cells (R3230Ac) were a gift from Dr. Mark Dewhirst (Duke University School of Medicine, North Carolina) (Hilf, Michel 1965, Lindberg, Dewhirst 1996). R3230Ac cells were thawed using a 37°C water bath, plated in cell culture T-75 flasks (Greiner Bio-one, Monroe, CA) without the addition of matrix substrate and cultured in high glucose DMEM media (Invitrogen, Carlsbad, CA) with 10% Fetal Bovine Serum (Omega Scientific, Tarzana, CA) and 1% antibiotic-antimycotic (Invitrogen) until 80% confluent. Cells were harvested for animal injection using TrypLE Express cell dissociation enzyme (Invitrogen). Live cell concentration was determined using trypan blue and a hemacytometer. Cells were re-suspended in PBS at a concentration of $2\times l0^6$ cells/mL for injection.

In vivo study overview

This paper includes the results of 132 imaging studies (91 ultrasound acquisitions and 41 MRI sessions), studying a total of 21 animals.

NIH-PA Author Manuscript

NIH-PA Author Manuscript

NIH-PA Author Manuscript

Preliminary study for sample size calculation

All protocols were approved by the Institutional Animal Care and Use Committee (IACUC). A preliminary study (N=4) was performed to determine the required sample size for subsequent experiments. MRI and ultrasound were acquired with all animals receiving the drug AG-028262. Based on this study, we found that for a paired t-test (using each animal as its own control) with alpha of 0.05 and sigma of 0.1, we can detect a difference of 50% with a power approaching 1 (0.9755) with N=3. Our changes from preliminary studies indicated the change exceeded 50% in each case. Furthermore, the study involves repeated measures and therefore the power is higher than estimated above.

Additional studies involved a total of 17 (N=7 control, N=10 treated) animals which were bilaterally transplanted with tumors for imaging. All animals were evaluated with ultrasound at baseline and 24 hours post-treatment. Subsets of the treatment groups underwent evaluation using MRI, were tracked longitudinally for 3 weeks and/or were imaged in multiple planes to assess regional variation (Table 1).

Statistical Analysis

Statistical analysis was performed in consultation with the Division of Biostatistics at UC Davis Medical School using R and Excel (Microsoft, Redmond, WA). Significance for ultrasound replenishment times was determined using an unpaired two-sample t-test to compare control versus AG-028262 treatment regimens ($p<0.05$). Change from baseline and intra-tumoral regional variability was evaluated using a paired two-sample t-test ($p<0.05$). The primary analytic goal of the longitudinal study was to assess the trajectory of perfusion during a three week treatment interval and determine differences for treated mice. We fitted repeated-measures mixed-effect regression models (Diggle 2002, Laird and Ware 1982); these models allow for within-animal correlation due to characteristics of the animal. We included terms to test for an overall difference between treated and control mice, successive changes from week 1 to 2 and week 2 to 3, and possible differences within week. MRI replenishment rates were calculated using MATLAB to determine the slope of the MRI signal intensity data above and below the 80% signal intensity threshold. We assessed the degree to which ultrasound measures were associated with MRI tumor volume measurements using a repeated-measures mixed-effects linear model with MRI as outcome and ultrasound as predictor, to take account of possible within-animal correlation. The r^2 value was calculated using array analysis with the linest function for linear regression in Excel with y=mx (since MRI and ultrasound replenishment times will presumably never be zero).

Antiangiogenic drug treatment

The caudal flanks of three-week-old, male, Fischer344 rats (Harlan Laboratories, Hayward, CA) were injected with a single-cell suspension of 1×10^6 R3230Ac cells in 0.5 mL PBS. Imaging and antiangiogenic drug treatment commenced once a palpable tumor was identified (~0.5 cm in diameter). Animals were initially anesthetized in an induction chamber with 5% aerosolized isoflurane in oxygen. Anesthesia was maintained throughout the imaging study using titrated isoflurane/O^2 administered through a nose cone. The drug used in this study was AG-028262, a potent inhibitor of VEGF-R (VEGF-R1, -R2, and -R3) phosphorylation, provided by Pfizer Global Research (La Jolla, CA USA). AG-028262 is administered bi-daily, per-orally (BID, PO). In this study, animals received a one-day treatment of AG-028262 or diluent each week (60 mg/kg/day, two 30mg/kg doses given 8 hours apart) after pre-treatment images for ultrasound and MRI were obtained (day 0). Pre-treatment ultrasound imaging was performed prior to pre-treatment MRI imaging. Immediately following the pre-treatment MRI, animals were orally gavaged with either 0.5% carboxymethylcellulose (CMC, vehicle control media) or a suspension of AG-028262

NIH-PA Author Manuscript

NIH-PA Author Manuscript

NIH-PA Author Manuscript

in 0.5% CMC. Animals were re-imaged with MRI 24 hours after the first dosing and ultrasound images were acquired immediately following MRI acquisition. Eight of these animals (four control, four AG-028262) were treated weekly with AG-028262 or diluent for three weeks.

Ultrasound imaging protocol

Ultrasound imaging was performed by an experienced ultrasound technician. Vascular replenishment rates were measured using motion corrected CPS ultrasound. Ultrasound images were acquired using an Acuson Sequoia 512 system (Siemens Medical Solutions USA, Inc, Ultrasound Division, Issaquah, WA) with a 15L8 linear array transducer. Prior to ultrasound, the animals' caudal flank region was shaved and depilated using Veet (Reckitt Benckiser North America, Inc., Parsippany, NJ). The transducer was coupled to the surface of the skin with acoustic coupling gel (Aquasonic, Parker Laboratories, Fairfield, NJ). The area of each tumor was estimated using the elliptic caliper function in the sagittal plane of the tumor. Upon identifying the tumor's largest sagittal cross-sectional area, the transducer was mechanically fixed in position with an articulated arm. Definity (Bristol-Myers Squibb, N. Billerica, MA) was activated by shaking according to the manufacturer's instructions. Using a syringe pump (Harvard Apparatus, Holliston, MA), the contrast agent was infused at a concentration of 8×10^8 microbubbles/mL through a 24 gauge tail vein catheter with an injection port at a rate of 60 μL/min. The continuous-rate injection of microbubbles was initiated 1 minute prior to each imaging sequence to allow circulating contrast concentration to stabilize. Parametric maps of contrast replenishment were acquired in real-time using Siemens motion sensing probe (MSP) with CPS. MSP was applied to track regions affected by respiration-induced motion. After contrast concentration stabilization, a high mechanical index (MI) destructive pulse (5 MHz, 1.9 MI) cleared the sample volume of contrast agent. This was followed by a lower MI series of pulses (7 MHz, 0.28 MI) as the tumor was replenished. Automated MSP processing performed frame-to-frame alignment using a real-time sum of the absolute difference between B-mode images, and then further mapped the color of each pixel according to the time required to reach an intensity threshold set to 80% of full scale. The colormap is a nonlinear map designed to provide high sensitivity to small differences in fast blood flow (fast arrival time), and lower sensitivity to changes in slow blood flow (slow arrival time), approximately corresponding to the changes in flow velocity with vessel diameter. Final images were recorded and saved for further off-line processing to quantify replenishment in designated regions. Calculated replenishment times were an average of three image sequences per tumor.

Vascular density was estimated by the fraction of the tumor region of interest in the CPS images that was enhanced above the noise threshold, where 1 indicates 100%.

Intra-tumoral variability and repeatability of ultrasound imaging

Variability was assessed for three AG-028262-treated animals based on the image acquisition and animal preparation as described above. Image sets were acquired in multiple planes pre-treatment to establish baseline replenishment times, as well as 24 hours and 5 days post-treatment for each animal. The transducer was mechanically fixed in position with a 360-90/443/433 series manual positioning linear stage (Newport, Irvine, CA). Three destruction-replenishment image sequences were obtained after finding the largest sagittal cross-sectional tumor area. Two subsequent intra-tumoral regions were imaged using the same methodology after moving the transducer 2 mm to either side of the original position. Motion compensation was applied as described above.

NIH-PA Author Manuscript

NIH-PA Author Manuscript

NIH-PA Author Manuscript

Longitudinal study

Four animals receiving AG-028262 and four animals receiving 0.5% CMC (control) were monitored for three weeks (N=8). Animals received the drug or control treatment at the beginning of each week and where imaged 24 and 48 hours after dosing.

Post processing (ultrasound)

Captured parametric images were post-processed in MATLAB (Mathworks, Natick, MA). Regions of interest (ROIs) were manually drawn on B-mode tumor images and applied to the color parametric image. The time required for 80% replenishment was determined, and the mean value of the 80% replenishment time over the tumor region was determined for each imaging plane. Finally, the percent change in the time to 80% replenishment (T80%) was calculated between the pre- and post- treatment values for the entire tumor.

Tumor Growth

Tumor area was estimated using the equation: ellipse area = pi*a*b, where a= 0.5*major axis, b=0.5*minor axis. The major and minor axes were measured by using the elliptic caliper function on the Acuson Sequoia ultrasound system for the largest tumor cross-section in the sagittal plane. Due to inter-animal tumor growth rate and/or size variability, the percent change in area was calculated to reflect changes in tumor growth using the following equation:

$$\%\ \text{change in area} = [(2^{nd}\ \text{value} - 1^{st}\ \text{value})/1^{st}\ \text{value}] * 100$$

$$1^{st}\ \text{value} = \text{per-treatment area}$$

$$2^{nd}\ \text{value} = \text{area measured 24 or 48 hours after treatment}$$

Magnetic resonance imaging protocol

MRI images were obtained by an experienced MRI technician. Contrast-enhanced MRI was performed using a General Electric superconducting 1.5 Tesla, HiSpeed imaging system (Milwaukee, WI, USA). The anesthetized rat (weighing ~250 grams) was placed on the patient table and a T_1-weighted localizer sequence (TR 433.3 ms, TE 10.0 ms, slice thickness 2.0 mm) was initiated to identify the axial view containing the maximal tumor area with an arterial input. The identified slice was used to acquire a spoiled gradient recalled (SPGR) sequence (TR 21.0 ms, TE 6.0 ms, slice thickness 2.0 mm, 128 × 128 matrix). The field-of-view for the SPGR sequence was 4.0 × 4.0 cm^2 resulting in a spatial resolution of 0.31 × 0.31 mm^2. A pre-contrast agent image was obtained, followed by a 0.1 mmol/kg (0.2 mL gadolinium/kg) bolus injection of a gadolinium based contrast agent (Magnevist, Bayer HealthCare Pharmaceuticals, Wayne, NJ, USA) administered through a 24 gauge tail-vein catheter with an injection port. The administered gadolinium dose falls within the linear enhancement range (0-5.0 mmol/L for 1.5T MRI system) (Morkenborg, Pedersen 2003). The imaging technician administered 0.6 mL diluted gadolinium solution (0.8 Magnevist into 4.0 mLs sterile saline) over three seconds – the injection rate was matched between animals, but was injected manually. Images were then acquired every three seconds for the first two minutes and every 30 seconds for the remaining two minutes.

Post processing (MRI)

The average MRI signal intensity was processed using MATLAB. A fitted curve of MRI signal intensity versus time was produced using a moving average filter combining 5 equally-weighted contiguous time points. These filtered data points were normalized by subtracting the intensity before contrast injection, calculating the maximum intensity after

NIH-PA Author Manuscript

NIH-PA Author Manuscript

NIH-PA Author Manuscript

baseline subtraction, then dividing by this value to produce a curve ranging between 0 and 1. Normalized fitted data were then segmented according to the 80% cutoff. Linear regression was applied for values above and below the 80% normalized intensity and the slopes were determined.

Histology

Tumors were removed immediately after Euthasol-induced cardiac arrest. Tumors were bifurcated to permit proper overnight fixation in 10% Formalin. Once the tissue was fixed, tumors were transferred to 70% ethanol. After fixation, tumors were processed with a Tissue Tek VIP then paraffin embedded using a Tissue Tek TEC (Sakura Finetek, Torrence CA, USA). Four micron slices were cut using a manual rotary microtome (Leica RM2235, Leica Microsystems Inc., Bannockburn, IL USA) and stained with hematoxylin and eosin.

Results

Ultrasound

Intra-tumoral variability and repeatability—Replenishment times were evaluated across three planes of acquisition acquired before and after drug administration (Figure 1). The statistical significance of regional variability was analyzed for three image acquisitions in each of the three intra-tumoral para-sagittal planes. There was no statistical difference in the replenishment times calculated for the individual intra-tumoral regions (Figure 1); however, as expected, the effect of drug treatment was evident in all planes by the increased replenishment time at 24 hours and 5 days, as compared with the baseline ($p<0.05$).

Respiration, as observed within the tumor imaging frame, resulted in a mean and peak frame displacement of 0.34 and 0.52 mm, respectively, corresponding to a maximum displacement of 9 image pixels. Thus, estimates of contrast replenishment on a pixel-by-pixel basis required motion correction. Following motion correction, the standard deviation of the replenishment time was ±0.129 sec with the mean ranging from 0.2 to 5 seconds.

Drug efficacy—The baseline time to 80% replenishment and vascular density were similar for animals receiving control versus AG-028262 treatment (Figure 2A, 2C). The T80% for AG-028262-treated animals increased by 74% to 4.54 ± 0.9 sec 24 hours post therapy, while the T80% decreased by 13% to 2.7 ± 0.8 sec for control animals. At 48 hours post therapy, the T80% for AG-028262-treated animals remained elevated at 4.4 ± 1.7 sec, while the T80% increased slightly (Figure 2A) control animals. After this time, without further treatment, tumor re-growth occurred and the value returned to the original range. Parametric images (Figures 2D and 3) of control and AG-028262 tumors demonstrate the real-time system performance.

At 24 hours post treatment, the ultrasound-based estimate of vascular density for AG-028262 animals decreased to 0.4 ± 0.2, while the vascular density for control animals did not change significantly (0.8 ± 0.2), resulting in a significant difference between control and treated vascular densities (Figure 2B). Forty-eight hours after treatment, the vascular density for AG-028262 animals recovered (0.8 ± 0.2), while the density estimate for control animals remained stable (0.8 ± 0.1) (Figure 2B).

In a longitudinal study over three weeks, animals were dosed one day per week (with a concentration typically administered daily) and imaged before and after treatment to determine whether the imaging method would yield consistent and significant results as the tumor vasculature matures (Figures 2C, 2D, and 3). Longitudinal monitoring of the effect of AG-028262 over three weeks demonstrated a significant increase ($P<0.001$, repeated

NIH-PA Author Manuscript

NIH-PA Author Manuscript

NIH-PA Author Manuscript

measures calculation) in T80% after each treatment (Figures 2C, 2D, 3). Baseline T80% values for treated and control animals at weeks 1, 2 and 3 were similar, although the baseline decreased each week for both groups, likely due to vascular maturation. Week 1 baseline T80% for AG-028262-treated and control animals was 3.4 ± 1.4 sec and 3.4 ± 0.5 sec, respectively, and it increased 24 hours after dosing to 5.7 ± 0.6 sec for AG-028262-treated animals, but remained unchanged for control animals. On week 2, the baseline measures of T80% for both control and AG-028262-treated animals were comparable at 3.2 ± 0.4 sec and 2.9 ± 1.1 sec respectively. The T80% value elevated to 4.7 ± 0.9 sec 24 hours post AG-028262 treatment, but decreased to 2.7 ± 1.1 sec for control animals. At week 3, the baseline T80% values for AG-028262-treated and control animals were 2.9 ± 1.3 sec and 2.9 ± 1.0 sec, respectively. Twenty-four hours post treatment, T80% for AG-028262-treated animals increased to 4.4 ± 0.5 sec while the T80% for control animals decreased to 2.4 ± 0.52 sec. Parametric images for control and AG-028262-treated animals provide visual confirmation of the above results with fast replenishment times represented in yellow and slow in red (Figures 2D, 3). We find that the parametric images provide a rapid indication of therapeutic effect even for larger tumors with mature vasculature, with the reduction in fast flow indicated by the reduction in yellow pixels.

Tumor Growth—Tumor cross-sectional area, as assessed from B-mode ultrasound images, rapidly decreased after drug therapy. Twenty-four and 48 hours after administration, the area decreased by 5.6 ± 19.9% and 7.9 ± 9.5%, respectively (Figure 4A). Tumor cross sectional area for control animals reflected the rapid tumor growth, increasing at 24 hours by 6.5 ± 30.2% and by 21.9 ± 14.8% at 48 hours.

In the longitudinal study of one-day per-week therapy (Figure 4B), the tumor growth rate decreased in the AG-028262-treated animals, as evidenced by the tumor area of drug-treated animals increasing by 10.9 ± 10.8% by week 2 and 109.1 ± 34.5% by week 3. By comparison, the cross sectional area of control tumors increased by 43.9 ± 17.0% by week 2 and 174.3 ± 89.5% by week 3. Parametric images captured the differences in the growth pattern as monitored over the three-week duration (Figure 4C). As shown in detail in earlier papers, histological slices of control (Figure 4D) and AG-028262-treated (Figure 4E) tumors confirmed ultrasound size estimates (Chomas, Pollard 2003, Pollard, Garcia 2004).

Magnetic Resonance Imaging

Replenishment was estimated with both MRI and ultrasound in the same animals; a typical contrast-enhanced MRI image, with outlined bilateral tumors and gadolinium reference, is shown in Figure 5A. MRI data analysis was conducted using MATLAB to produce a fitted curve from the average intensity versus time measurements (Figure 5B). The slope was calculated using linear regression analysis (Figure 5C), and the inverse of the slope was used to estimate the perfusion time. Antiangiogenic treatment resulted in a decreased rate of perfusion (Figure 6A) while control values were relatively stable (Figure 6B). Baseline T80% values for control and AG-028262 animals were not significantly different (23.7±2.4 sec versus 29.5±13.0 sec respectively) and MRI perfusion time increased with AG-028262-treatment (Figure 6C). While the perfusion time increased slightly in control animals 24 hours post treatment (33.4±5.2 sec), a significant difference was observed between control and AG-028262-treated animals at 24 hours after treatment (50.8±28.4 sec with $p<0.03$). Increased ultrasound levels were strongly associated with significant increases in MRI measure, with a 0.20 unit increase in MRI on average for each unit increase in US ($P=0.003$). MRI versus ultrasound replenishment times ($n = 40$) demonstrate a positive linear correlation between the two imaging modalities ($r^2 = 0.86$ for Figure 6D).

NIH-PA Author Manuscript

NIH-PA Author Manuscript

NIH-PA Author Manuscript

Discussion and Summary

Motion-corrected destruction-replenishment CPS ultrasound offers noninvasive, real-time analysis of antiangiogenic treatment efficacy. The task of mapping vessels in tumors with ultrasound has previously been difficult because the tumor attenuates the ultrasound wave and the acoustic echoes from blood can be 34-40 dB below those of the surrounding walls. Ultrasound detection of tumors and the characterization of the vascular function within tumors are used in clinical applications, including the detection of lesions in the breast, prostate, thyroid, liver, and the skin. Transrectal ultrasound has been used in prostate screening for diagnosis, biopsy guiding and treatment (Nelson, Slotoroff 2007, Nelson, Slotoroff 2007). Without a contrast agent, large vessels that are visualized with ultrasound have not shown adequate specificity in the differentiation of benign and malignant lesions. Also, for interventions such as radio frequency ablation (RFA) or ultrasonic ablation, ultrasound is already being used and is far more convenient for monitoring response. With the addition of contrast agents, ultrasound is sensitive to capillary-sized vessels and very low flow rates while maintaining the ability to detect morphological information from traditional B-mode imaging. Contrast ultrasound has the potential to assess individual responses to antiangiogenic therapy. Recent studies indicate that the loss of VEGF signaling and the induction of a hypoxic environment may increase angiogenesis, neovascularization and metastasis through compensatory mechanisms (Du, Lu 2008, Ebos, Lee 2009, Paez-Ribes, Allen 2009). As tumors evolve to be drug resistant, it is important to develop technology that can provide real-time, non-invasive, serial images to assess tumor progression and perfusion.

Our previous work in the development of methods to quantify microvascular flow rate (Chomas, Pollard 2003) led us to develop and test destruction-replenishment algorithms for the assessment of antiangiogenic therapies (Broumas, Pollard 2005, Pollard, Broumas 2007, Pollard, Garcia 2004) using subharmonic filtering to distinguish tissue and microbubble echoes. We have previously shown that the morphology of ultrasound maps and histology are highly correlated (Broumas, Pollard 2005, Chomas, Pollard 2003, Pollard 2002). By quantifying the time for replenishment resulting from destruction-replenishment, we are quantifying a relative measure that should be independent of gain and attenuation. The time to replenishment is not a classical physiological parameter, as compared with the flow rate measures described by Wei and others (Unger, McCreery 1998, Wei, Ragosta 2001), but the measurement is robust in the presence of attenuation, amenable to real-time mapping and demonstrates changes with therapy (Figure 3). Methods of destruction-replenishment imaging based on physiological models for volume flow require use of the image amplitude (Wei, Jayaweera 1998), whereas the replenishment time method applied here is independent of amplitude and therefore gain. We find that such replenishment time estimates simply and reliably detect changes with therapy. However, a disadvantage of destruction-replenishment strategies is the requirement for high-pressure destructive pulses. Within the United States, current trials of ultrasound contrast imaging for radiology applications do not include high MI pulses. Furthermore, we apply a constant infusion over several minutes to achieve a consistent contrast agent concentration in blood; however, we recognize that with normalization for contrast agent circulation, bolus injection can be applied in such studies (Averkiou, Lampaskis 2010, Hoyt, Warram 2010).

Most importantly, in our study, the time required for tumor contrast replenishment was significantly greater after antiangiogenesis treatment than at baseline, and therefore therapeutic response can be assessed by the replenishment time without calculating the change over treatment. This is useful for extended clinical studies of therapeutic efficacy where it may be difficult to register ultrasound planes over successive studies. Compared with methods that use only low-pressure ultrasound pulses, the destruction-replenishment

NIH-PA Author Manuscript

NIH-PA Author Manuscript

NIH-PA Author Manuscript

methods used here simplify processing by isolating the measurement of flow rate to the tumor vasculature. Variations in the local replenishment rate of the contrast agent across the tumor, or before and after treatment, are independent of the systemic cardiac dynamics. Since repeated examinations will likely result in assessment in different planes, we studied whether inter-plane variability will affect measured values. As shown in Figure 1, the difference in para-sagittal plane analysis does not significantly alter the results.

The nonlinear map, corresponding to the changes in flow rate as a function of vessel diameter, enhanced the recognition of region boundaries and flow rate quantization. Images are color coded according to the time required for replenishment of the contrast agent within the tumor. The nonlinear color scale facilitates immediate visualization of mature vasculature and changes in vascular morphology with treatment. With such mapping, ultrasound can assess treatment-based modulation of small versus large vessels and high volume versus low volume flow facilitating controlled timing for chemotherapy and other combination therapies.

The Siemens Sequoia was used in this study for two reasons: first, the transmitter matches the inverted pulses with high precision and creates a very high contrast-to-tissue ratio image; second, the Sequoia has two parallel processing pathways, where one pathway can be used for gray scale image alignment (i.e. real-time motion correction) and the second can be used for flow processing. The embedded Sequoia algorithm uses CPS for the rejection of tissue echoes, rather than the subharmonic strategies used previously (Pollard, Dayton 2009); however, CPS may produce a higher signal-to-noise ratio than the subharmonic mode with the bandwidth available on current transducers.

Imaging of angiogenesis has been investigated using magnetic resonance imaging with and without a contrast agent. Many MR-based techniques have been explored including those that assess flow, vascular permeability and vascular maturity (Marcus, Ladam-Marcus). DCE-MRI is arguably the gold standard for evaluating tumor response (Chou, Wu 2007, Marcus, Ladam-Marcus). Moreover, Brasch et al. suggest that MRI is sensitive enough to detect acute changes in tumor microvascular permeability after a single dose of therapy (Brasch and Turetschek 2000, Chou, Wu 2007, Wilmes, Pallavicini 2007). However, MRI is expensive and gadolinium agents can be toxic in patients with renal disease. In addition, quantifying perfusion with MRI is complicated by the need for an arterial input function, a known contrast agent injection rate, and the need for the concentration of contrast agent to be in the linear enhancement range (Yankeelov, DeBusk 2006). Furthermore, analyzing the first hundred seconds of MRI data limited the extravasation of MR contrast agents (Yankeelov, Niermann 2006). Ultrasound replenishment measurements have substantial advantages as compared to MR, computed tomography, and positron emission tomography (PET). First, in many cases, ultrasound can improve spatial resolution and assess very slow flow. Second, ultrasound utilizes a purely intravascular tracer, and therefore compartmental analysis is not required. Microbubble contrast agents provide a direct measurement of blood flow, volume and local velocity. Alternatively, a change in perfusion may affect the evaluation of metabolism by PET, and a change in absolute blood flow may affect the estimate of vascular permeability by MR or CT. An estimate of vascular density also changed significantly with drug therapy; however, this estimate is dependent on establishing an amplitude threshold for the contrast echoes and can be difficult in the presence of attenuation and noise.

Another benefit of using the destruction-replenishment scheme described here is that flow rate can be repeatedly measured within a single examination and the variance of the estimator can be reduced. This is not possible with MR and CT contrast agents, even with macromolecular agents. A high spatial resolution is achievable due to the use of a higher

NIH-PA Author Manuscript

NIH-PA Author Manuscript

NIH-PA Author Manuscript

frequency (7 MHz) and is desirable for superficial organs such as breast and prostate. With the addition of contrast agents, ultrasound is sensitive to capillary-sized vessels and very low flow rates while maintaining the ability to detect morphological information from traditional B-mode imaging, giving this modality the sensitivity to detect and monitor cancer progression and treatment (Gore, Yankeelov 2009). Furthermore, assessment of tumor replenishment (in contrast to assessing plasma concentrations or vascular permeability) may be the most relevant end point for assessing the activity of antiangiogenic agents or effects of such agents on the delivery of chemotherapy to tumors (Saleem and Price 2008). Finally, the relative cost-effectiveness, lower cost and portability of ultrasonographic equipment make ultrasound an attractive imaging modality to monitor the activity of angiogenesis inhibitors such as VEGF-R inhibitors in the clinic.

Acknowledgments

We appreciate the support of NIH R01CA103838, NIH R01CA134659, and the Biostatistics Shared Resource of the UC Davis Cancer Center Grant P30CA093373-06. We thank Rich Larson for performing the MRI studies, Jennifer Fung for assisting in experimental studies, Dr. Laurel Beckett for statistical assistance and advice and Pfizer Oncology for providing the drug.

References

Averkiou M, Lampaskis M, Kyriakopoulou K, Skarlos D, Klouvas G, Strouthos C, Leen E. Quantification of tumor microvascularity with respiratory gated contrast enhanced ultrasound for monitoring therapy. Ultrasound Med Biol. 2010; 36:68–77. [PubMed: 19900749]

Bartels E, Henning S, Wellmer A, Giraldo-Velasquez M, Kermer P. Evaluation of cerebral perfusion deficit in stroke patients using new transcranial contrast imaging CPS technology--preliminary results. Ultraschall Med. 2005; 26:478–86. [PubMed: 16453219]

Bauditz J, Schade T, Wermke W. Sonographic diagnosis of hilar cholangiocarcinomas by the use of contrast agents. Ultraschall Med. 2007; 28:161–7. [PubMed: 17366374]

Bohs LN, Trahey GE. A novel method for angle independent ultrasonic imaging of blood flow and tissue motion. IEEE Trans Biomed Eng. 1991; 38:280–6. [PubMed: 2066142]

Brasch R, Turetschek K. MRI characterization of tumors and grading angiogenesis using macromolecular contrast media: status report. European Journal of Radiology. 2000; 34:148–55. [PubMed: 10927157]

Broumas AR, Pollard RE, Bloch SH, Wisner ER, Griffey S, Ferrara KW. Contrast-enhanced computed tomography and ultrasound for the evaluation of tumor blood flow. Investigative Radiology. 2005; 40:134–47. [PubMed: 15714088]

Calamante F, Vonken EJ, van Osch MJ. Contrast agent concentration measurements affecting quantification of bolus-tracking perfusion MRI. Magn Reson Med. 2007; 58:544–53. [PubMed: 17763347]

Chomas JE, Dayton P, Allen J, Morgan K, Ferrara KW. Mechanisms of contrast agent destruction. IEEE Trans Ultrason Ferroelectr Freq Control. 2001; 48:232–48. [PubMed: 11367791]

Chomas JE, Pollard RE, Sadlowski AR, Griffey SM, Wisner ER, Ferrara KW. Contrast-enhanced US of microcirculation of superficially implanted tumors in rats. Radiology. 2003; 229:439–46. [PubMed: 14526091]

Chou CP, Wu MT, Chang HT, Lo YS, Pan HB, Degani H, Furman-Haran E. Monitoring Breast Cancer Response to Neoadjuvant Systemic Chemotherapy Using Parametric Contrast-Enhanced MRI: A Pilot Study. Academic Radiology. 2007; 14:561–73. [PubMed: 17434070]

Dayton PA, Ferrara KW. Targeted imaging using ultrasound. J Magn Reson Imaging. 2002; 16:362–77. [PubMed: 12353252]

Diggle, P. Analysis of longitudinal data. Oxford ; New York: Oxford University Press; 2002.

Dijkmans PA, Knaalpen P, Aiazian E, Visser CA, Lammertsma AA, Visser FC, Kamp O. Myocardial perfusion as measured with real-time myocardial contrast echocardiography in healthy volunteers

NIH-PA Author Manuscript

NIH-PA Author Manuscript

NIH-PA Author Manuscript

correlates with positron emission tomography. Circulation. 2004; 110:718–18. [PubMed: 15289381]

Du R, Lu KV, Petritsch C, Liu P, Ganss R, Passegue E, Song H, Vandenberg S, Johnson RS, Werb Z, Bergers G. HIF1alpha induces the recruitment of bone marrow-derived vascular modulatory cells to regulate tumor angiogenesis and invasion. Cancer Cell. 2008; 13:206–20. [PubMed: 18328425]

Ebos JM, Lee CR, Cruz-Munoz W, Bjarnason GA, Christensen JG, Kerbel RS. Accelerated metastasis after short-term treatment with a potent inhibitor of tumor angiogenesis. Cancer Cell. 2009; 15:232–9. [PubMed: 19249681]

El Khouli RH, Macura KJ, Barker PB, Habba MR, Jacobs MA, Bluemke DA. Relationship of temporal resolution to diagnostic performance for dynamic contrast enhanced MRI of the breast. J Magn Reson Imaging. 2009; 30:999–1004. [PubMed: 19856413]

Elkington AG, He T, Gatehouse PD, Prasad SK, Firmin DN, Pennell DJ. Optimization of the arterial input function for myocardial perfusion cardiovascular magnetic resonance. J Magn Reson Imaging. 2005; 21:354–9. [PubMed: 15779035]

Ellis LM, Reardon DA. Cancer: The nuances of therapy. Nature. 2009; 458:290–2. [PubMed: 19295595]

Feinstein SB. The powerful microbubble: from bench to bedside, from intravascular indicator to therapeutic delivery system, and beyond. Am J Physiol Heart Circ Physiol. 2004; 287:H450–7. [PubMed: 15277188]

Foster FS, Burns PN, Simpson DH, Wilson SR, Christopher DA, Goertz DE. Ultrasound for the visualization and quantification of tumor microcirculation. Cancer Metastasis Rev. 2000; 19:131–8. [PubMed: 11191052]

Gore JC, Yankeelov TE, Peterson TE, Avison MJ. Molecular imaging without radiopharmaceuticals? J Nucl Med. 2009; 50:999–1007. [PubMed: 19443583]

Harrer JU, Hornen S, Oertel MF, Stracke CP, Klotzsch C. Comparison of perfusion harmonic imaging and perfusion mr imaging for the assessment of microvascular characteristics in brain tumors. Ultraschall Med. 2008; 29:45–52. [PubMed: 18098091]

Hilf R, Michel I, Bell C, Freeman JJ, Borman A. Biochemical and Morphologic Properties of a New Lactating Mammary Tumor Line in the Rat. Cancer Res. 1965; 25:286–99. [PubMed: 14281095]

Horsfield MA, Thornton JS, Gill A, Jager HR, Priest AN, Morgan B. A functional form for injected MRI Gd-chelate contrast agent concentration incorporating recirculation, extravasation and excretion. Phys Med Biol. 2009; 54:2933–49. [PubMed: 19384006]

Hoyt K, Warram JM, Umphrey H, Belt L, Lockhart ME, Robbin ML, Zinn KR. Determination of breast cancer response to bevacizumab therapy using contrast-enhanced ultrasound and artificial neural networks. J Ultrasound Med. 2010; 29:577–85. [PubMed: 20375376]

Jiang J, Hall TJ. A parallelizable real-time motion tracking algorithm with applications to ultrasonic strain imaging. Phys Med Biol. 2007; 52:3773–90. [PubMed: 17664576]

Kholmovski EG, DiBella EV. Perfusion MRI with radial acquisition for arterial input function assessment. Magn Reson Med. 2007; 57:821–7. [PubMed: 17457875]

Krix M, Plathow C, Kiessling F, Herth F, Karcher A, Essig M, Schmitteckert H, Kauczor HU, Delorme S. Quantification of perfusion of liver tissue and metastases using a multivessel model for replenishment kinetics of ultrasound contrast agents. Ultrasound in Medicine and Biology. 2004; 30:1355–63. [PubMed: 15582235]

Laird NM, Ware JH. Random-effects models for longitudinal data. Biometrics. 1982; 38:963–74. [PubMed: 7168798]

Lamuraglia M, Escudier B, Chami L, Schwartz B, Leclere J, Roche A, Lassau N. To predict progression-free survival and overall survival in metastatic renal cancer treated with sorafenib: pilot study using dynamic contrast-enhanced Doppler ultrasound. Eur J Cancer. 2006; 42:2472–9. [PubMed: 16965911]

Larsson HB, Stubgaard M, Sondergaard L, Henriksen O. In vivo quantification of the unidirectional influx constant for Gd-DTPA diffusion across the myocardial capillaries with MR imaging. J Magn Reson Imaging. 1994; 4:433–40. [PubMed: 8061444]

NIH-PA Author Manuscript

NIH-PA Author Manuscript

NIH-PA Author Manuscript

Lassau N, Brule A, Chami L, Benatsou B, Peronneau P, Roche A. Evaluation of early response to antiangiogenic treatment with dynamic contrast enhanced ultrasound. J Radiol. 2008; 89:549–55. [PubMed: 18535495]

Lassau N, Chami L, Benatsou B, Peronneau P, Roche A. Dynamic contrast-enhanced ultrasonography (DCE-US) with quantification of tumor perfusion: a new diagnostic tool to evaluate the early effects of antiangiogenic treatment. Eur Radiol. 2007; 17 6:F89–98. [PubMed: 18376462]

Lassau N, Chebil M, Chami L, Bidault S, Girard E, Roche A. Dynamic contrast-enhanced ultrasonography (DCE-US): a new tool for the early evaluation of antiangiogenic treatment. Target Oncol. 2010; 5:53–8. [PubMed: 20379790]

Lassau N, Lamuraglia M, Chami L, Leclere J, Bonvalot S, Terrier P, Roche A, Le Cesne A. Gastrointestinal stromal tumors treated with imatinib: monitoring response with contrast-enhanced sonography. AJR Am J Roentgenol. 2006; 187:1267–73. [PubMed: 17056915]

Li PC, Lee WN. An efficient speckle tracking algorithm for ultrasonic imaging. Ultrason Imaging. 2002; 24:215–28. [PubMed: 12665238]

Lindberg RA, Dewhirst MW, Buckley BJ, Hughes CS, Whorton AR. Ca(2+)-dependent nitric oxide release in endothelial but not R3230Ac rat mammary adenocarcinoma cells. Am J Physiol. 1996; 271:C332–7. [PubMed: 8760062]

Magnon C, Galaup A, Rouffiac V, Opolon P, Connault E, Rose M, Perricaudet M, Roche A, Germain S, Griscelli F, Lassau N. Dynamic assessment of antiangiogenic therapy by monitoring both tumoral vascularization and tissue degeneration. Gene Ther. 2007; 14:108–17. [PubMed: 16943854]

Marcus CD, Ladam-Marcus V, Cucu C, Bouché O, Lucas L, Hoeffel C. Imaging techniques to evaluate the response to treatment in oncology: Current standards and perspectives. Critical Reviews in Oncology/Hematology. In Press, Corrected Proof.

Meves SH, Wilkening W, Thies T, Eyding J, Holscher T, Finger M, Schmid G, Ermert H, Postert T. Comparison between echo contrast agent-specific imaging modes and perfusion-weighted magnetic resonance imaging for the assessment of brain perfusion. Stroke. 2002; 33:2433–7. [PubMed: 12364734]

Morkenborg J, Pedersen M, Jensen FT, Stodkilde-Jorgensen H, Djurhuus JC, Frokiaer J. Quantitative assessment of Gd-DTPA contrast agent from signal enhancement: an in-vitro study. Magn Reson Imaging. 2003; 21:637–43. [PubMed: 12915195]

Nelson ED, Slotoroff CB, Gomella LG, Halpern EJ. Targeted Biopsy of the Prostate: The Impact of Color Doppler Imaging and Elastography on Prostate Cancer Detection and Gleason Score. Urology. 2007; 70:1136–40. [PubMed: 18158034]

Nelson ED, Slotoroff CB, Gomella LG, Halpern EJ. Targeted biopsy of the prostate: the impact of color Doppler imaging and elastography on prostate cancer detection and Gleason score. Urology. 2007; 70:1136–40. [PubMed: 18158034]

Niermann KJ, Fleischer AC, Huamani J, Yankeelov TE, Kim DW, Wilson WD, Hallahan DE. Measuring tumor perfusion in control and treated murine tumors: correlation of microbubble contrast-enhanced sonography to dynamic contrast-enhanced magnetic resonance imaging and fluorodeoxyglucose positron emission tomography. J Ultrasound Med. 2007; 26:749–56. [PubMed: 17526606]

O'Connor JP, Carano RA, Clamp AR, Ross J, Ho CC, Jackson A, Parker GJ, Rose CJ, Peale FV, Friesenhahn M, Mitchell CL, Watson Y, Roberts C, Hope L, Cheung S, Reslan HB, Go MA, Pacheco GJ, Wu X, Cao TC, Ross S, Buonaccorsi GA, Davies K, Hasan J, Thornton P, del Puerto O, Ferrara N, van Bruggen N, Jayson GC. Quantifying antivascular effects of monoclonal antibodies to vascular endothelial growth factor: insights from imaging. Clin Cancer Res. 2009; 15:6674–82. [PubMed: 19861458]

O'Connor JP, Jackson A, Parker GJ, Jayson GC. DCE-MRI biomarkers in the clinical evaluation of antiangiogenic and vascular disrupting agents. Br J Cancer. 2007; 96:189–95. [PubMed: 17211479]

Padhani AR, Husband JE. Dynamic contrast-enhanced MRI studies in oncology with an emphasis on quantification, validation and human studies. Clin Radiol. 2001; 56:607–20. [PubMed: 11467863]

NIH-PA Author Manuscript

NIH-PA Author Manuscript

NIH-PA Author Manuscript

Paez-Ribes M, Allen E, Hudock J, Takeda T, Okuyama H, Vinals F, Inoue M, Bergers G, Hanahan D, Casanovas O. Antiangiogenic therapy elicits malignant progression of tumors to increased local invasion and distant metastasis. Cancer Cell. 2009; 15:220–31. [PubMed: 19249680]

Phillips P, Gardner E. Contrast-agent detection and quantification. Eur Radiol. 2004; 14 8:P4–10. [PubMed: 15700327]

Pollard R, Sadlowski AR, Bloch SH, Murray L, Wisner ER, Griffey S, Ferrara KW. Contrast-assisted destruction-replenishment ultrasound for the assessment of tumor microvasculature in a rat model. Technol Cancer Res Treat. 2002; 1:459–70. [PubMed: 12625773]

Pollard RE, Broumas AR, Wisner ER, Vekich SV, Ferrara KW. Quantitative contrast enhanced ultrasound and CT assessment of tumor response to antiangiogenic therapy in rats. Ultrasound in Medicine and Biology. 2007; 33:235–45. [PubMed: 17306694]

Pollard RE, Dayton PA, Watson KD, Hu X, Guracar IM, Ferrara KW. Motion corrected cadence CPS ultrasound for quantifying response to vasoactive drugs in a rat kidney model. Urology. 2009; 74:675–81. [PubMed: 19589583]

Pollard RE, Garcia TC, Stieger SM, Ferrara KW, Sadlowski AR, Wisner ER. Quantitative evaluation of perfusion and permeability of peripheral tumors using contrast-enhanced computed tomography. Investigative Radiology. 2004; 39:340–49. [PubMed: 15167100]

Potdevin TC, Fowkes JB, Moskalik AP, Carson PL. Analysis of refill curve shape in ultrasound contrast agent studies. Medical Physics. 2004; 31:623–32. [PubMed: 15070263]

Saleem A, Price PM. Early tumor drug pharmacokinetics is influenced by tumor perfusion but not plasma drug exposure. Clin Cancer Res. 2008; 14:8184–90. [PubMed: 19088034]

Tofts PS, Brix G, Buckley DL, Evelhoch JL, Henderson E, Knopp MV, Larsson HBW, Lee TY, Mayr NA, Parker GJM, Port RE, Taylor J, Weisskoff RM. Estimating kinetic parameters from dynamic contrast-enhanced t1-weighted MRI of a diffusable tracer: Standardized quantities and symbols. Journal of Magnetic Resonance Imaging. 1999; 10:223–32. [PubMed: 10508281]

Tweedle MF, Wedeking P, Telser J, Sotak CH, Chang CA, Kumar K, Wan X, Eaton SM. Dependence of MR signal intensity on Gd tissue concentration over a broad dose range. Magn Reson Med. 1991; 22:191–4. discussion 95-6. [PubMed: 1812345]

Unger EC, McCreery TP, Sweitzer RH, Caldwell VE, Wu YQ. Acoustically active lipospheres containing paclitaxel - A new therapeutic ultrasound contrast agent. Investigative Radiology. 1998; 33:886–92. [PubMed: 9851823]

von Herbay A, Schick D, Horger M, Gregor M. Low-MI-sonography with the contrast-agent SonoVue in the diagnosis of infarction of the spleen, kidney, liver and pancreas. Ultraschall Med. 2006; 27:445–50. [PubMed: 17033946]

Wei K, Jayaweera AR, Firoozan S, Linka A, Skyba DM, Kaul S. Quantification of myocardial blood flow with ultrasound-induced destruction of microbubbles administered as a constant venous infusion. Circulation. 1998; 97:473–83. [PubMed: 9490243]

Wei K, Le E, Bin JP, Coggins M, Thorpe J, Kaul S. Quantification of renal blood flow with contrast-enhanced ultrasound. Journal of the American College of Cardiology. 2001; 37:1135–40. [PubMed: 11263620]

Wei K, Ragosta M, Thorpe J, Coggins M, Moos S, Kaul S. Noninvasive quantification of coronary blood flow reserve in humans using myocardial contrast echocardiography. Circulation. 2001; 103:2560–65. [PubMed: 11382724]

Wilmes LJ, Pallavicini MG, Fleming LM, Gibbs J, Wang D, Li KL, Partridge SC, Henry RG, Shalinsky DR, Hu-Lowe D, Park JW, McShane TM, Lu Y, Brasch RC, Hylton NM. AG-013736, a novel inhibitor of VEGF receptor tyrosine kinases, inhibits breast cancer growth and decreases vascular permeability as detected by dynamic contrast-enhanced magnetic resonance imaging. Magnetic Resonance Imaging. 2007; 25:319–27. [PubMed: 17371720]

Wink MH, de la Rosette JJ, Laguna P, Lagerveld BW, Wijkstra H. Ultrasonography of renal masses using contrast pulse sequence imaging: a pilot study. J Endourol. 2007; 21:466–72. [PubMed: 17523897]

Wink MH, Laguna MP, Lagerveld BW, de la Rosette JJ, Wijkstra H. Contrast-enhanced ultrasonography in the follow-up of cryoablation of renal tumours: a feasibility study. BJU Int. 2007; 99:1371–5. [PubMed: 17355368]

NIH-PA Author Manuscript

NIH-PA Author Manuscript

NIH-PA Author Manuscript

Yankeelov TE, Cron GO, Addison CL, Wallace JC, Wilkins RC, Pappas BA, Santyr GE, Gore JC. Comparison of a reference region model with direct measurement of an AIF in the analysis of DCE-MRI data. Magnetic Resonance in Medicine. 2007; 57:353–61. [PubMed: 17260371]

Yankeelov TE, DeBusk LM, Billheimer DD, Luci JJ, Lin PC, Price RR, Gore JC. Repeatability of a reference region model for analysis of murine DCE-MRI data at 7T. J Magn Reson Imaging. 2006; 24:1140–7. [PubMed: 17024660]

Yankeelov TE, Niermann KJ, Huamani J, Kim DW, Quarles CC, Fleischer AC, Hallahan DE, Price RR, Gore JC. Correlation between estimates of tumor perfusion from microbubble contrast-enhanced sonography and dynamic contrast-enhanced magnetic resonance imaging. J Ultrasound Med. 2006; 25:487–97. [PubMed: 16567438]

Zhu Y, Hall TJ. A modified block matching method for real-time freehand strain imaging. Ultrason Imaging. 2002; 24:161–76. [PubMed: 12503771]

Zou HY, Li Q, Grazzini M, Dillon R, Amundson K, Acena A, Wickman G, Shelley A, Rewolinski D, Jacobs S, Solowiej J, Murray B, McTigue M, Romines W, Lou J, Gale D, Bender S, Kania R, Shalinsky DR, Hu-Lowe DD. AG-028262, a novel selective VEGFR tyrosine kinase antagonist that potently inhibits KDR signaling and angiogenesis in vitro and in vivo. AACR Meeting Abstracts. 2004; 2004:595–c-.

NIH-PA Author Manuscript

NIH-PA Author Manuscript

NIH-PA Author Manuscript

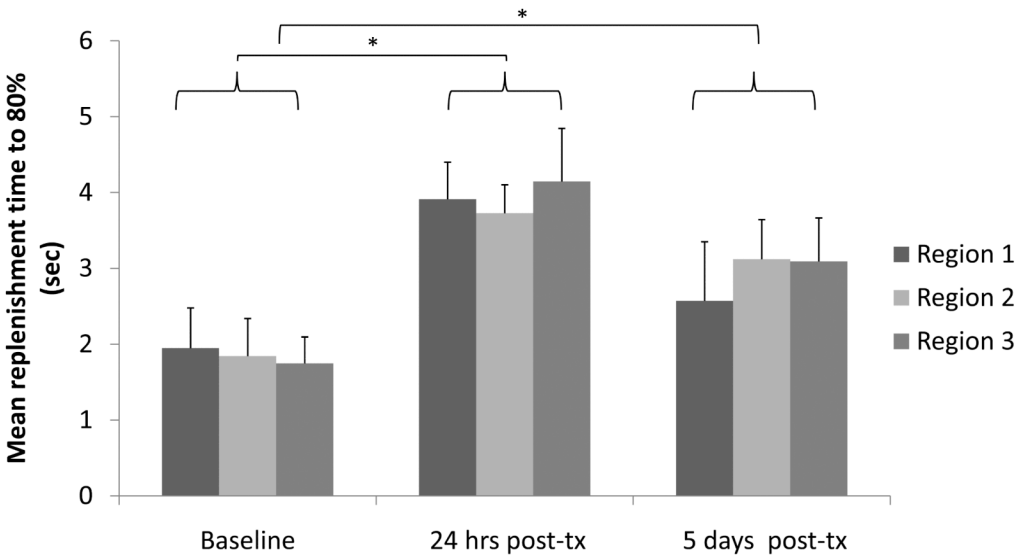

Figure 1.

Comparison of T80% replenishment time for three sagittal and para-sagittal planes, demonstrating the repeatability of measurements. (* indicates significance with $p \leq 0.05$). Each column is an average of three image acquisitions for three animals.

NIH-PA Author Manuscript
NIH-PA Author Manuscript
NIH-PA Author Manuscript

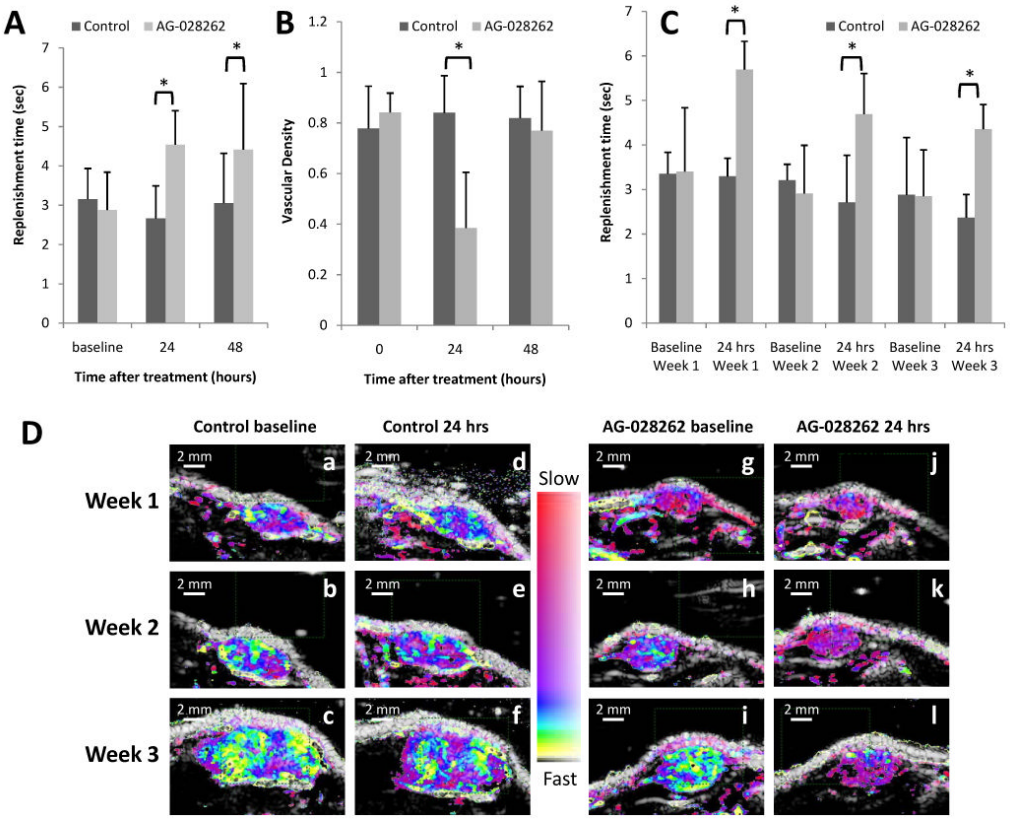

Figure 2. VEGF-R drug effect on T80% replenishment time and vascular density

A) Ultrasound measure of replenishment times. Replenishment rates at baseline are equivalent for drug versus control animals, but the antiangiogenic effect of the drug is evident at 24 and 48 hours after drug administration as demonstrated by the increase in replenishment time (* indicates significance with $p \leq 0.05$). **B)** Ultrasound estimates of vascular density. Ultrasound can be used to predict vascular density by estimating the percent of tumor region of interest filled with contrast echoes. We show that the animals receiving the antiangiogenic drug tend to have a decrease in vascular density (* indicates significance with $p \leq 0.05$). **C)** Three-week overview of replenishment time. Each column represents a mean of four animals. For each animal we acquired triplicate imaging sequences that were averaged. While replenishment time increases for animals receiving AG-028262 at 24 hours, the effect is not as great at weeks 2 and 3 possibly due to previous drug exposure (* indicates significance with $p \leq 0.05$). **D)** Parametric destruction-replenishment images of control (a-f) and AG-028262 (g-l) animals for baseline (a-c and g-i) versus 24 hours (d-f and j-l) post diluent and drug administration.

NIH-PA Author Manuscript

NIH-PA Author Manuscript

NIH-PA Author Manuscript

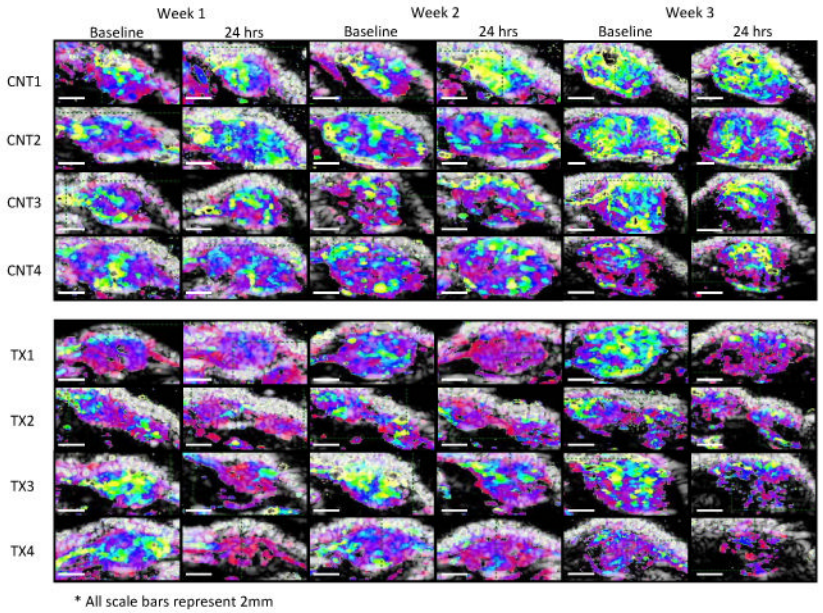

Figure 3. Longitudinal parametric images

Three-week overview of the ultrasound replenishment times and tumor growth for control versus treated animals at baseline and 24 hours post oral gavage.

NIH-PA Author Manuscript

NIH-PA Author Manuscript

NIH-PA Author Manuscript

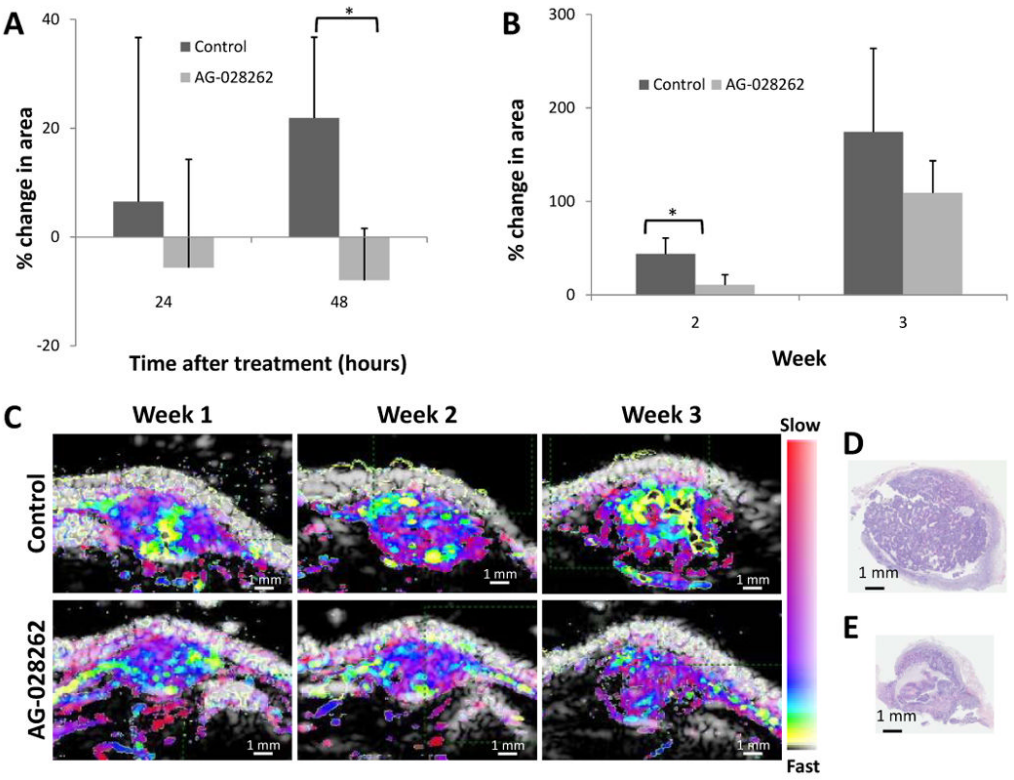

Figure 4. Efficacy of tumor therapy assessed by tumor area

A) Post treatment tumor growth showing the percent change in area 24 and 48 hours after treatment. Control tumors continue to develop while AG-028262 induces tumor regression (* indicates significance with $p \leq 0.05$). **B)** Weekly percent change in area from week 1 to weeks 2 and 3. There is a significant decrease in tumor growth rate for animals receiving AG-028262 by week 2. The trend is still apparent by week 3 (* indicates significance with $p \leq 0.05$). **C)** Comparison (a-f) for control (a-c) vs. drug (d-f) over a 3 week interval. **D)** H&E of control RATMAC tumor at the end of a 3 week study. **E)** H&E of RATMAC tumor from an animal receiving one weekly dose of AG-028262 for 3 weeks confirming the repression of growth as shown in ultrasound.

NIH-PA Author Manuscript

NIH-PA Author Manuscript

NIH-PA Author Manuscript

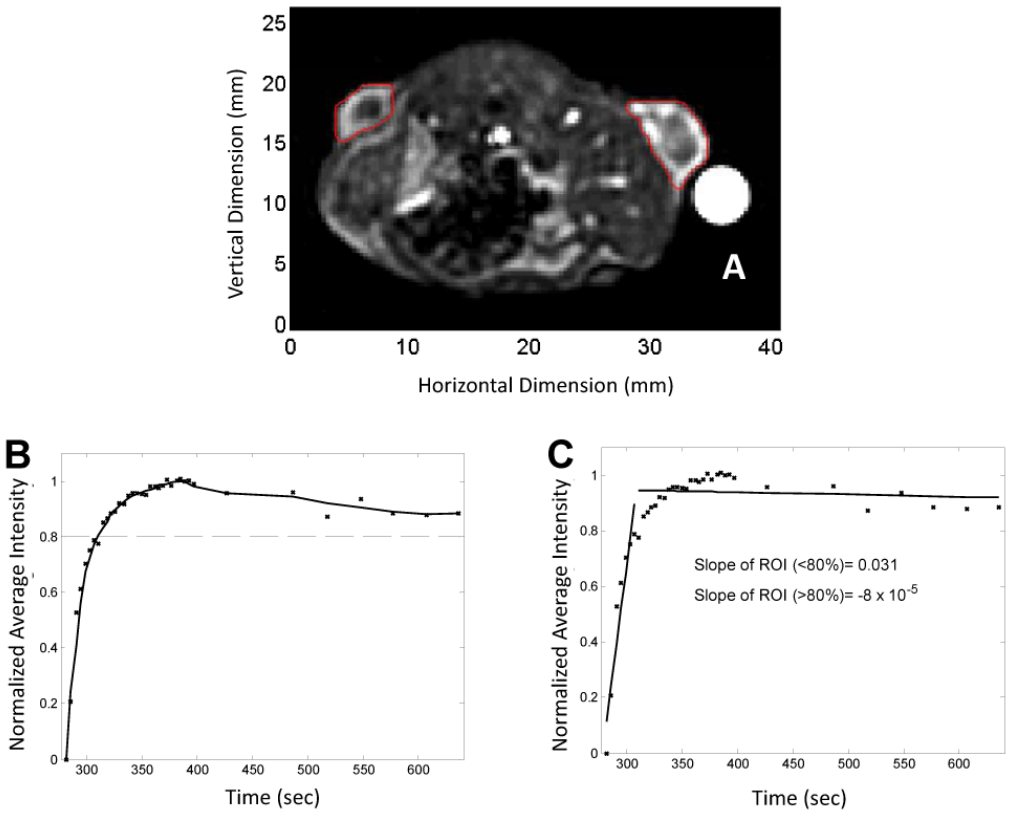

Figure 5. MRI sample data and image

A) Representative example of an MRI acquisition with region of interests drawn around the left and right tumors. **B)** MRI SPGR signal intensity vs time. **C)** Linear Regression. The slope of the average intensity for the tumor is computed using a linear regression model. With successful treatement, the slope decreases. The inverse slope is calculated to examine the perfusion rate.

NIH-PA Author Manuscript

NIH-PA Author Manuscript

NIH-PA Author Manuscript

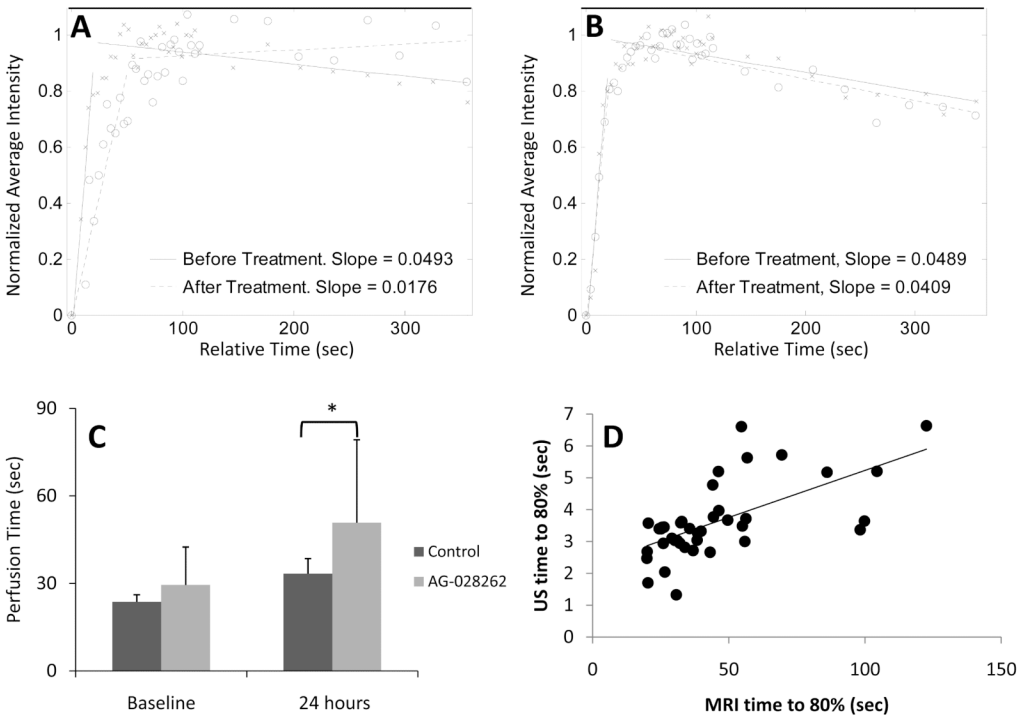

Figure 6. Results of MRI analysis

A) Linear regression analysis for a representative AG-028262 animal before and 24 hours after drug administration. **B)** Linear regression analysis for a representative control animal before and 24 hours after treatment. **C)** Average MRI Perfusion times. Time to 80% perfusion for control versus animals receiving AG-028262 demonstrates a significant difference at 24 hours post treatment (* indicates significance with $p \leq 0.05$). **D)** Two-modality correlation. Graphing the time to 80% replenishment for the two modalities shows a significant, positive linear correlation.

NIH-PA Author Manuscript

NIH-PA Author Manuscript

NIH-PA Author Manuscript

Table 1
Number of animals used for in vivo studies

	Baseline + 24 hrs (ultrasound)	Baseline + 24 hrs (MRI)	Longitudinal	Multi-plane
Control	7	4	4	
Treated (AG-028262)	10	9	4	3

A total of 17 animals were used in this study with subsets of those animals used for MRI perfusion analysis, longitudinal drug effect, and multi-plane replenishment evaluation.